Sedimentary Geology 360 (2017) 22–34

Contents lists available at ScienceDirect

Sedimentary Geology

journal homepage: www.elsevier.com/locate/sedgeo

On the origin of silt laminae in laminated shales

Zalmai Yawar *, Juergen Schieber

Department of Geological Sciences, Indiana University, United States

ARTICLE INFO

Article history:
Received 26 May 2017
Received in revised form 31 August 2017
Accepted 1 September 2017
Available online 06 September 2017

Editor: Dr. B. Jones

Keywords:
Laminated mudstone
Flocculated clay
Silt laminae
Mudstone deposition
Depositional fabric
Bedload transport

ABSTRACT

Experiments with mixtures of quartz silt and clays, under conditions where pure silt and clay suspensions form bedload ripples (non-cohesive silt, flocculated clay) show that coarse silt does segregate from clays during transport. As bedload transport proceeds, ripples of coarse silt and flocculated mud migrate over the bed surface simultaneously. Migrating ripples leave behind a thin veneer of silt grains or clay floccules, and over time a laminated deposit, consisting of thin parallel silt and clay laminae, builds up. If silt of a wide size range (60 μm to a few microns) is used, the coarse silt ends up in ripples and silt laminae, whereas the fine silt (20 μm or less) is integrated into clay floccules and stays mixed and suspended in the flocculated clay matrix. In natural laminated mudstones, coarse silt is typically found in thin laminae, whereas fine silt occurs mainly in the interlaminated clays. These experiments produce an analogous particle distribution and therefore suggest a likely way in which laminated mudstones of the rock record were formed.

1. Introduction

The rock record is resplendent with laminated shales (e.g. Ulmer-Scholle et al., 2015) that owe their laminated nature to the presence of parallel laminae of coarse silt (dominantly 30–63 μm) that are interspersed with laminae of finer material (Fig. 1). When looked at in detail, there are multiple types of laminae in shales that are a reflection of a range of depositional settings (e.g. O'Brien, 1996). In this paper the focus is on thin silt laminae with sharp bottom and top contacts, and how they relate in terms of depositional conditions to overlying and underlying clay-rich layers. Though long thought to largely reflect distal deposition under quiescent and oxygen deprived conditions (e.g. Potter et al., 1980; Lundegard and Samuels, 1980; Cluff, 1980; Nuhfer, 1981), more recent flume experiments have shown an alternative mode for the formation of laminated shales. In these experiments, clay suspensions, propelled by swift currents (~20–25 cm/s; flow depth 5 cm), formed floccules that transferred to bedload, gave rise to migrating ripples, and accreted under flow into cm-thick mud beds (Schieber et al., 2007). These mud beds consisted of multiple overriding ripples, and because of high initial water content (~85 vol%) took on a laminated appearance after drying and compaction of the sediment. Careful examination of these beds still showed low-angle downlapping of internal laminae, and analogous examples from the rock record (Fig. 2) suggested that parallel laminae in shale may simply look parallel because they are so highly compacted (Schieber et al., 2007; Schieber and Southard, 2009; Schieber and Yawar, 2009; Schieber, 2011). There are, however, many laminated shales in the rock record, with discontinuous (Fig. 3) to continuous silt laminae that may extend decimeters and even meters across cut samples and outcrops (Fig. 4), much longer than the observed lateral extent of foreset laminae in the migrating ripples. In addition, such shales may largely lack low-angle downlapping relationships that would indicate that the laminae once were ripple foresets. Although we are confident that these laminae also owe their origin to bedload transport of mud, to achieve a better understanding of the underlying processes and conditions seemed advisable.

To this end we designed flume experiments that could potentially answer these questions. Because natural muds are not pure clay suspensions and typically contain silt grains that range in size from a few to 63 μm, we were curious whether suspensions that included clay and silt would show behavior similar to that of pure clay suspensions. Although there have been prior experimental studies of bedload transport and ripple formation in silt-size sediments (e.g. Rees, 1966; Mantz, 1978; Jopling and Forbes, 1979), we wanted to be sure to understand the behavior of the pure quartz silts at the experimental and flow conditions that were used in prior clay-only experiments. For the remainder of this manuscript, "silt" is implied to mean quartz silt of the type shown in Section 3.1.

Silt experiments show that each size grade has specific velocity ranges at which ripples are stable, and that these velocity ranges coincide with those where clay floccule ripples occurred in previous experiments. When silt and clay were mixed, an interesting phenomenon occurred – the sediment segregated during bedload transport, and two ripple types formed: (1) ripples made from coarse silt, and (2) ripples composed of clay floccules. Both ripple types were mobile at the same

* Corresponding author.
E-mail address: zyawar@indiana.edu (Z. Yawar).

http://dx.doi.org/10.1016/j.sedgeo.2017.09.001
0037-0738/

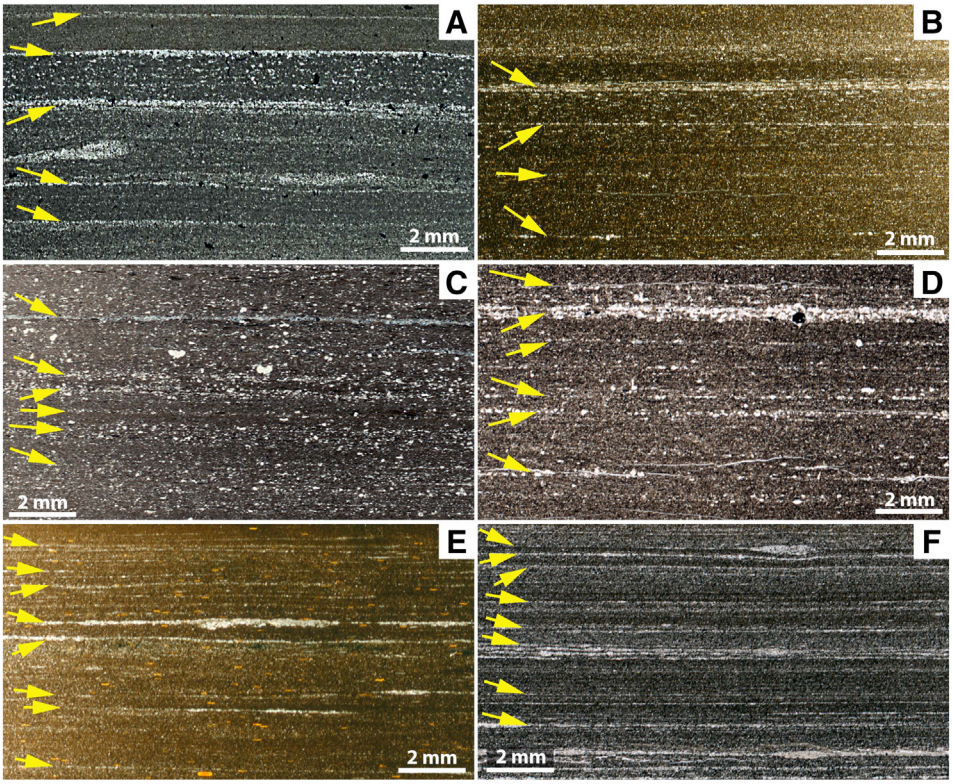

Fig. 1. A sampling of parallel-laminated shales from the rock record. Yellow arrows point to silt laminae. Note that there are many more very faint laminae spaced at sub-mm distances. A – Green River Fm., Eocene, Wyoming. B - Power Steps Fm., Ordovician, Newfoundland. C – Eagle Ford Shale, Cretaceous, Texas. D – Bakken Shale, Devonian, Saskatchewan. E – New Albany Shale, Devonian, Indiana. F – Chattanooga Shale, Devonian, Tennessee. (For interpretation of the references to colour in this figure legend, the reader is referred to the web version of this article.)

time and travelled over the flume bed together. At low sedimentation rates, individual ripples left behind a thin veneer of sediment as they passed over a given location in the flume, and as time went by a mud bed built up that consisted of randomly interspersed clay and coarse silt laminae. Scanning electron microscope (SEM) examination of epoxy stabilized and ion milled sediment samples from these experiments showed that the fine silt component (~1–30 μm) is intermingled with and "hidden" among clay minerals that were deposited as floccules, whereas the coarse silt laminae largely lack a clay-mineral component. Comparison with silt-laminated shales from the rock record shows a comparable distribution of silt grains between silt laminae and clay-dominated laminae. Our experiments show that alternating muddy and silt-rich laminae in a shale should not be taken as an indication of alternating currents and quiet interludes, but rather indicate bedload transport of mud by currents that may have been of considerable duration.

2. Methods

All of our experiments were carried out in a racetrack flume as described from previous studies (e.g. Schieber et al., 2007). The flume channel is 25 cm wide, the turning sections have a radius of 1.5 m, and the straight sections are 7.2 m long (Fig. 5). In order to have uniform

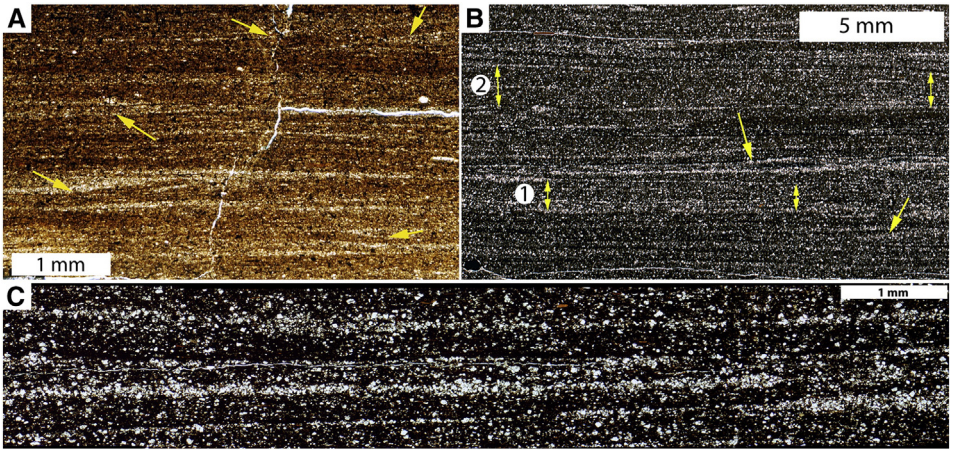

Fig. 2. Subtle cross-lamination and convergent laminae. (A) Photomicrograph of Mowry Shale (Cretaceous) with low-angle ripple lamination (arrows). Photo courtesy of Joe Macquaker. (B) Photomicrograph of Chattanooga Shale (Devonian) with low-angle ripple lamination and downlapping laminae (arrows). Double arrows mark laminae bundles that show lateral thinning, another indication of compacted cross-lamination. (C) Another example of lamina convergence in a probably ripple-laminated black shale (Chattanooga Shale, Devonian).

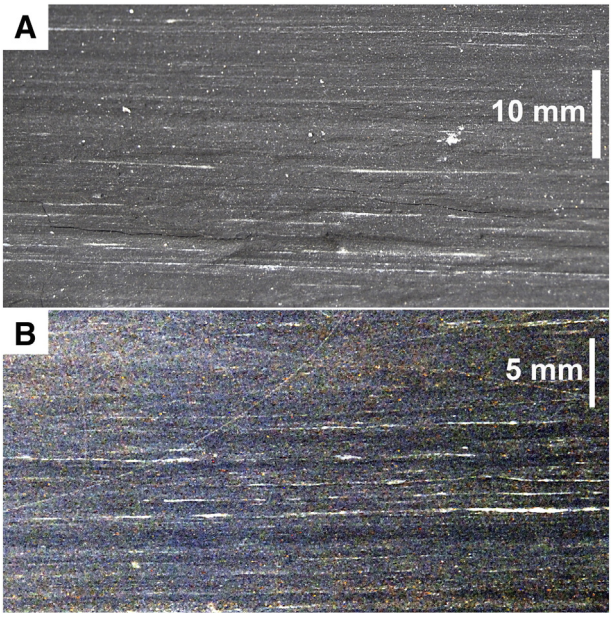

Fig. 3. Discontinuous silt laminae in the Devonian New Albany Shale. (A) is an outcrop image, and (B) is from a cut block.

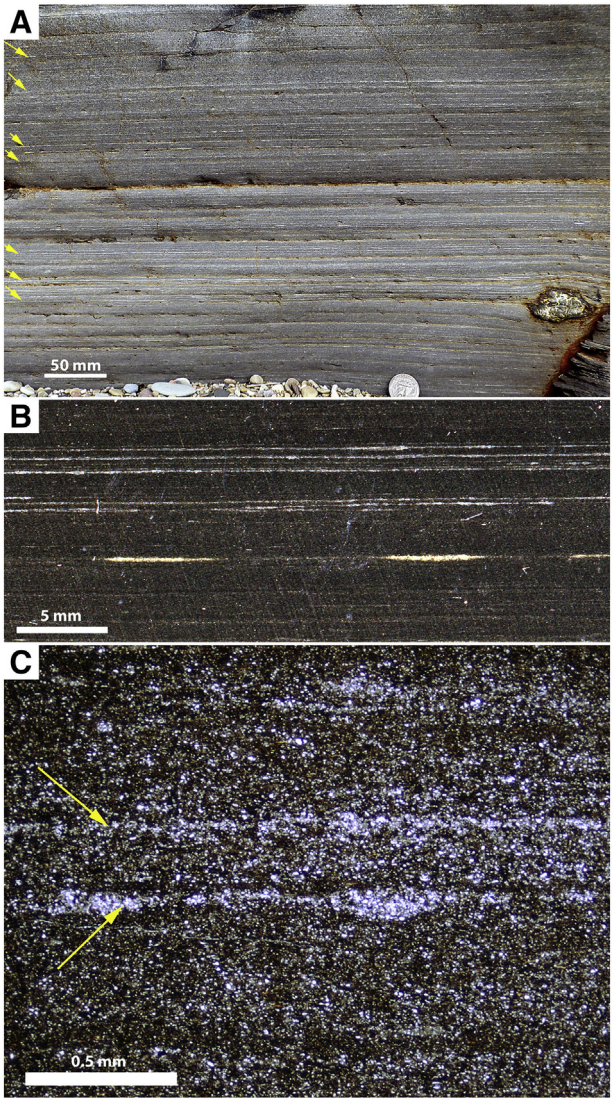

Fig. 4. Parallel laminae without indications of low-angle lamination and downlaps. (A) From outcrop of Devonian Dunkirk Shale, New York. Numerous sub-mm silt laminae (yellow arrows) can be followed across the outcrop for distances of as much as several meters. (B) Parallel continuous as well as discontinuous silt laminae in hand specimen of the Devonian New Albany Shale of Kentucky. (C) A closer look at silt laminae (arrows) from A (photomicrograph, transmitted light). Note thickening of silt laminae into lenses. "Thin" portions of these laminae may only be a few silt grains thick. As a result, these laminae may appear discontinuous in hand specimen or outcrop. (For interpretation of the references to colour in this figure legend, the reader is referred to the web version of this article.)

shear stress across the length of the flume, a flow lid is placed 10 cm above the flume bottom, and the water is moved by means of a paddle belt instead of a centrifugal pump. When muddy suspensions are propelled by the latter, any existing floccules are destroyed and the suspension is no longer in a "natural" state. The benefit of using a paddle belt is that the turbulence of the flow is probably not greatly different from what one would encounter in a river or tidal channel, floccules can persist in the flow, and the mixture can reach a "near natural" equilibrium between flocculation and dispersion (Schieber, 2011).

For the study of quartz-silt behavior, commercially available (vendor US Silica) quartz powders with top sizes of 50, 40, 30, and 5 μm were used (Fig. 6). The clays for mixed clay-silt experiments were commercially available Georgia kaolinite (vendor Thiele Kaolin) and illite clays (vendor Natural Sourcing). The high degree of angularity of these quartz grains (Fig. 7) is comparable to the angularity of detrital quartz silt from mudstones in the rock record (e.g. Schieber et al., 2000; Milliken et al., 2007; Schieber, 2009) and is thought to reflect the fact that silt grains tend to travel in suspension for a large part of their journey (Potter et al., 1980; Blatt, 1982). In addition, owing to the relatively low mass of silt-size quartz grains very little energy is expended when they collide during transport (e.g. Haines and Mazullo, 1988; Pye, 1994). Rounding of quartz silt grains that may be observed in thin section tends to be due to post-depositional diagenetic overgrowth (e.g. Schieber et al., 2000).

For each grade of quartz powder, there is a substantial proportion of material finer than the top size (Fig. 7). This "fine fraction" of each sediment batch was removed in an initial experiment step by continuously draining suspended sediment as the flume was running at 30 cm/s velocity until the recirculated fluid showed little residual turbidity.

After removing the "fine tail" of the commercially available size grades, the pure-silica experiments were conducted as follows. After initial suspension of the sediment at a flow velocity of 55 cm/s, the velocity was gradually reduced in increments of 5 cm/s, to determine at what velocity ripple formation occurs for a given size grade. The reported velocity data were measured 5 cm above the flume bottom with a Marsh-McBirney Flowmate 2 instrument, which measures flow using the Faraday law of electromagnetic induction. The flume channel design with a flow lid ensures uniform flow depth and a stable velocity profile, and thus flow velocity is measured at the effective flow depth (5 cm) of the system. Initially, after the introduction of the sediments into the flume, the flume was run at 55 cm/s velocity (to allow for thorough mixing of all grain sizes). After a few hours (minimum of 3 h runtime for each step) the velocity was reduced by a 5 cm/s increment. This process was repeated for all of the four grade sizes of silica until the velocity was at 10 cm/s, and the first occurrence of bedload ripples as well as the velocity at which ripple migration stopped was recorded. A time-lapse camera was used to record the experiments, complemented by visual observations of sediment movement and acquisition of HD camcorder movies. Still pictures of different stages of ripple movement were also taken. A sample was collected from bedload sediment (ripples) for later grain size verification by SEM once the finer fraction of the sample had been removed (drained).

Once the behavior of pure quartz silt size grades in our flume context had been established, we expanded the experiments to include

Fig. 5. Indiana University Flume Lab and the flume used for conducting the quartz-silt and quartz-clay-mixed experiments.

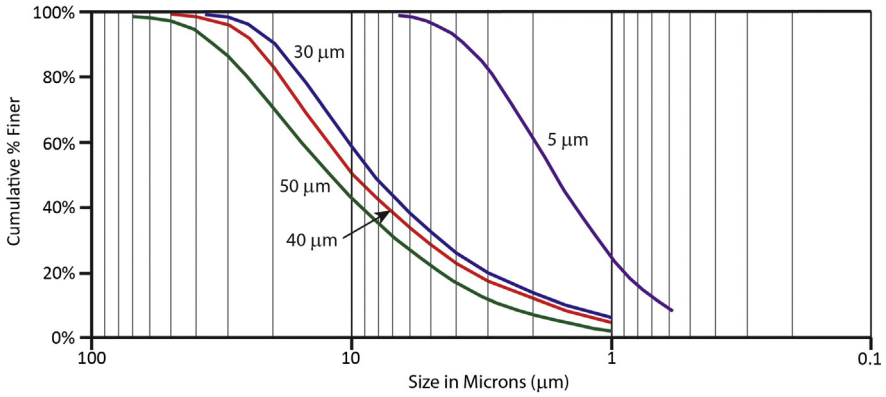

Fig. 6. Grain size distribution in commercially available quartz powders (US Silica) used in experiments (data provided by vendor). Note the broad size distributions. For the 50 µm powder used in the silt-clay experiments, 70% of the sample is finer than 20 µm, and 45% is finer than 10 µm.

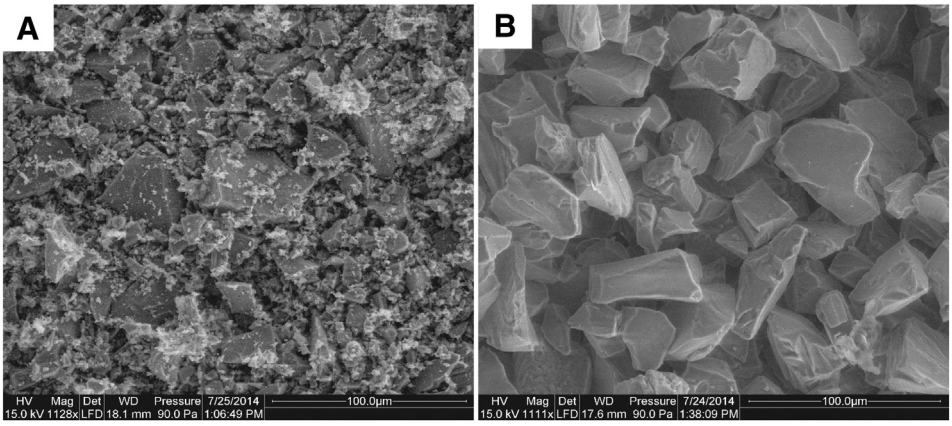

Fig. 7. The 50 µm size grade quartz silt (SEM images) before (A) and after (B) the finer components were removed. Note via reference to Fig. 6 that the bulk of the sample consists originally (A) of substantially smaller grain sizes.

Table 1
Quartz grain size and the flow velocity at which ripple formation starts and ripple migration ends.

Table 1	Ripple migration vs grain size	
Quartz grain size (µm)	Ripple formation starts (cm/s)	Ripple migration stops (cm/s)
50	55	15
40	40	10
30	40	10
5	20	10

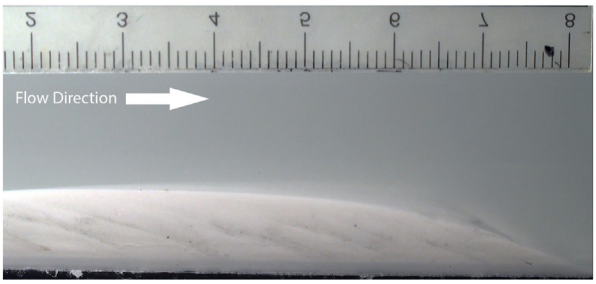

Fig. 8. Cross section of silt ripple (30 µm grain size) that migrated against the flume wall. Flow was from left to right, and darker impurities make internal cross laminae visible. The scale divisions are in mm, numbers mark cm, subdivisions.

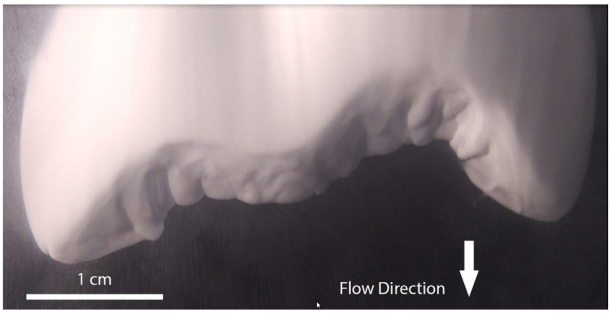

Fig. 9. Top view of the downstream end of a silt ripple that consists largely of 30 μm quartz (flow velocity 25 cm/s). Note the lobes of avalanching sediment on the downstream slip-face of the ripple.

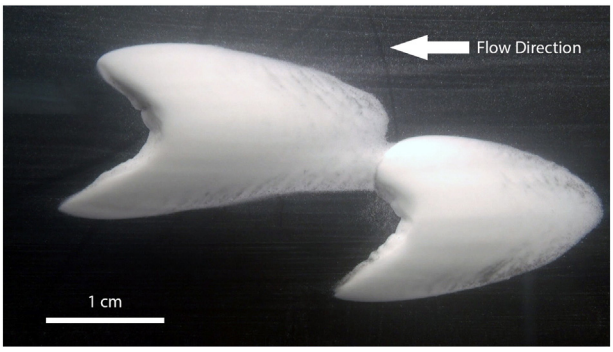

Fig. 10. Barchan-shaped silt ripples, flow from right to left (40 μm quartz; 25 cm/s). Note downcurrent-pointing horns and rounded upcurrent margin.

mixtures of quartz silt with kaolinite and quartz silt with illite. In both of the mixed quartz silt and kaolinite and the quartz silt and illite experiments, the sediment was introduced to the flume in three stages. At the first stage, 500 g of 5 μm quartz silt was introduced to the flume followed by 1000 g of kaolinite. The flow velocity was kept at 50 cm/s to allow for a thorough mixing of quartz silt and kaolinite. After 4 h of running the flume at 50 cm/s, the velocity was reduced to 20 cm/s (below the critical velocity of sedimentation for kaolinite, Schieber et al., 2007). A second batch of sediment, 500 g of 50 μm (top size) quartz silt mixed with 1000 g of kaolinite was added to the flume 24 h later (flow velocity remained at 20 cm/s). A final batch of 500 g of 50 μm quartz silt mixed with 1000 g of kaolinite was added to the flume 48 h after the second sediment addition in order to build up a thicker bed for later sampling and textural studies (flow velocity remained at 20 cm/s). Prior to addition of the final batch of sediment, 100 g of hematite dust (jewelers rouge) was also added to the flume to serve as a marker between the second and third sediment batch. Over the course of these experiments, a piston sampler (attached to the bottom of the flume) was gradually retracted (0.635 mm/h) in order to record the changing type of sediments that travelled across the flume bottom in the course of the experiment. The piston samples were sub-cored after conclusion of a given experiment, the cores embedded in Spurr resin, and then argon ion-milled, and examined by SEM for textural details. Although the images shown here are from experiments with freshwater suspensions, we did a set of saltwater experiments (3.5% salinity) to ascertain that under previously established experimental conditions there was no significant difference in the way the experiments proceeded and in the type of deposits that accumulated.

3. Observations

Observations made on pure silt, pure clay, and mixed silt-clay experiments are reported below. In addition SEM observations of grain size and texture of final deposits of mixed experiments are reported in a separate section.

3.1. Observations on silt ripples

Ripples produced from 30, 40, and 50 μm quartz powders behaved like sand ripples, and formed over a range of flow velocities (Table 1).

Particles moved up on the stoss side of the ripple and then avalanched down from the ripple crest and formed foresets (Fig. 8). Cross-sectional views of ripples can be observed when ripples migrate against the wall of the flume and reveal internal cross-laminae due to sediment avalanching down the lee side of the ripple (Fig. 9). Ripples that form below the upper limit of ripple formation (Table 1) are well defined barchans and have downcurrent-pointing horns and a rounded upcurrent margin (Fig. 10). As flow velocity is lowered after initial ripple formation, the migrating ripples gradually form a thin ribbon of sediment that lags behind the ripples and in effect constitutes a thin lamina of just a few grains thickness (Fig. 11).

These ripple "tails" expand in length as flow velocity is lowered towards the lower limit of ripple migration (Table 1) and may persist for the entire length of the flume channel (Fig. 12). In effect, these ripple "tails" form thin veneers of silt that eventually may be a thin silt lamina in a larger volume of sediment. The formation of these veneers is a critical element of the research that is presented here.

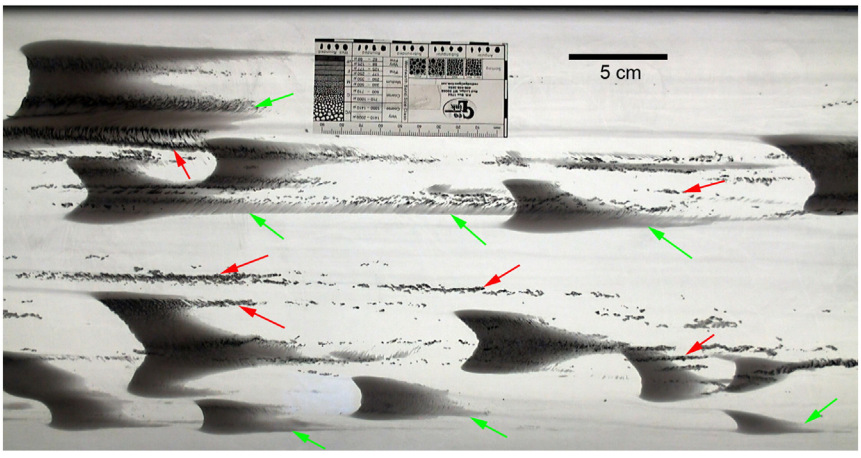

Fig. 11. Silt ripples migrating from right to left (30 μm quartz; 20 cm/s, view from below). Ripples have developed upcurrent-extending sediment "tails" (green arrows) and are migrating over the remains of older ripple tails (red arrows). (For interpretation of the references to colour in this figure legend, the reader is referred to the web version of this article.)

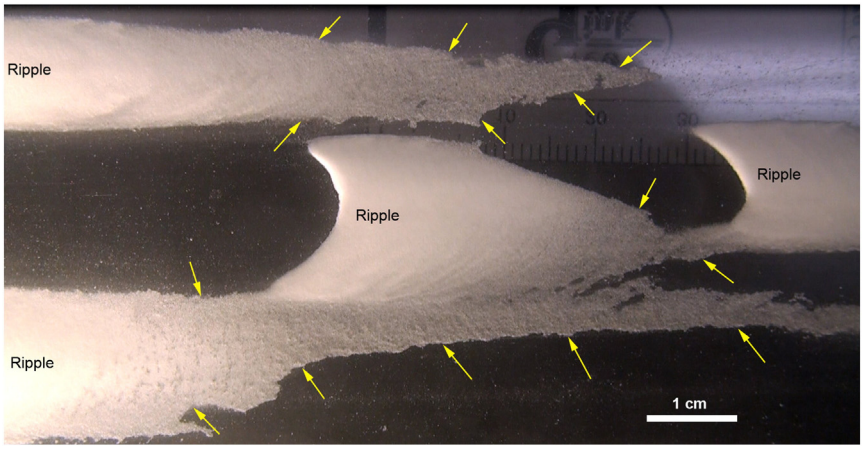

Fig. 12. Migrating coarse-silt ripples (50 μm quartz; 20 cm/s, flow from right to left), photographed from above. The yellow arrows point to residual sediment veneer that stays behind after the ripples pass. (For interpretation of the references to colour in this figure legend, the reader is referred to the web version of this article.)

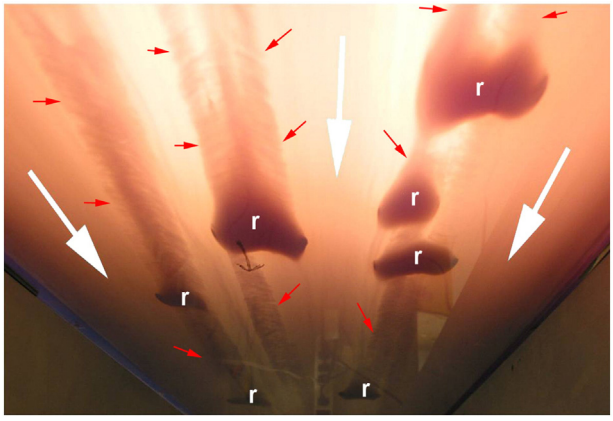

Fig. 13. Bottom view of the transparent flume channel. Flow direction is indicated by white arrows; flume channel width is 25 cm. The letter "r" marks migrating floccule ripples, and the red arrows mark clay tails that are left behind after ripples pass over the surface. (For interpretation of the references to colour in this figure legend, the reader is referred to the web version of this article.)

Depending on the rate of sediment delivery to the bed (sedimentation rate) different ripple morphologies formed in the silt experiments performed for this project. At comparatively small sedimentation rates barchans ripples are the common ripple morphology observed. At high sedimentation rates, achieved when the flow velocity is reduced quickly to the lower end of the flow velocity range shown in Table 1, transverse ripples form initially and then rearrange into barchans over time.

3.2. Observations on clay-floccule ripples

Although it has been long thought that deposition of muds and clays requires quiescent environments (e.g., Potter et al., 2005), multiple publications of recent flume experiments demonstrate that clays and muds can be deposited from turbid suspensions that move at flow velocities that would suffice to transport and deposit sand (Schieber et al., 2007; Schieber and Southard, 2009; Schieber, 2011). In these experiments flocculated clays and muds form floccule ripples that accrete into mud beds at flow velocities between 0.1 and 0.3 m/s. Bedload floccules typically are larger than 100 μm and may reach several 100 μm in size (Schieber et al., 2007; Schieber, 2011). As in the case of aforementioned silt ripples, ripple morphology can range from barchan to transverse as a consequence of sedimentation rates, and as flow velocities are lowered the migrating ripples leave behind a thin veneer of sediment (Fig. 13).

3.3. Observations on silt-clay mixed experiments

The objective of our experiments was to see how mixtures of quartz silt and clays behaved under the flow conditions previously explored for

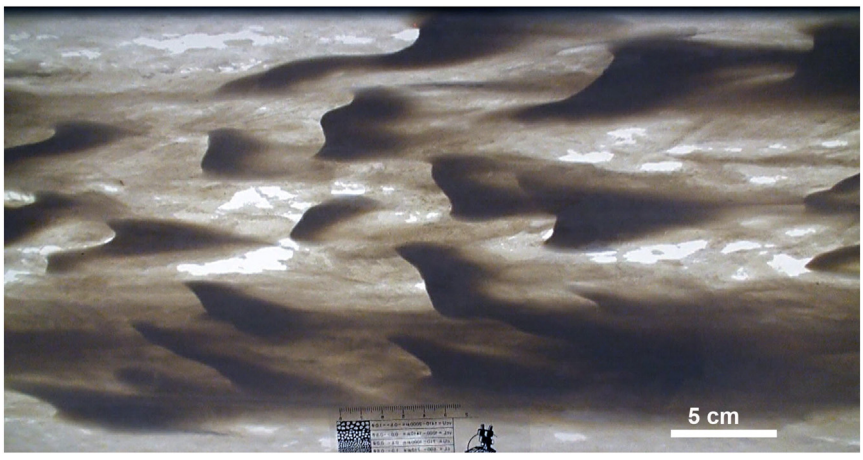

Fig. 14. Migrating ripples in a silt-illite experiment. Flow from right to left, photographed from below. Sediment veneers have covered most of the flume bottom, and with passage of more ripples the bed thickens (becomes darker).

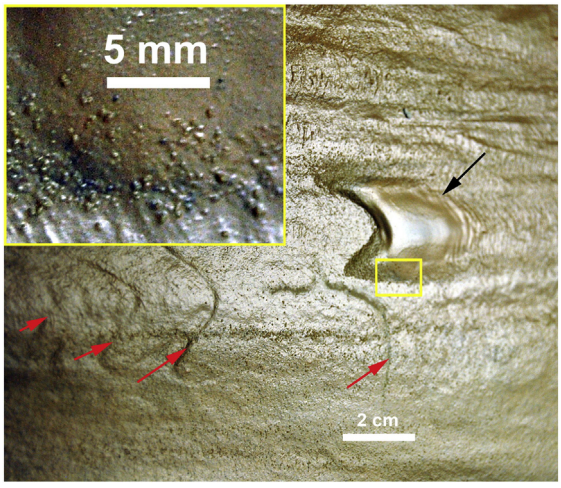

Fig. 15. Surface of the final (semi-dried) deposit from a silt-illite experiment. The more prominent (uncompacted) ripples consist of coarse quartz silt (black arrow), and the more subdued (compacted) ripples consist of flocculated illite (red arrows). Inset in the upper left corner is an enlargement of the lower flank of a silt ripple, and shows floccules that range in size from 100 to 500 μm. (For interpretation of the references to colour in this figure legend, the reader is referred to the web version of this article.)

bedload deposition of flocculated clays (Schieber et al., 2007; Schieber and Southard, 2009). The sediment mixtures consisted of quartz silt with 50 μm top size, and illite or kaolinite, and after conclusion of experimental runs the water was gently drained from the flume to avoid disruptions to the accumulated mud bed. In all flume runs, observations through the flume bottom (e.g. Schieber, 2011) showed travelling bedload particles of silt to sand size (clay floccules) that formed ripples and migrated in a downstream direction. This direct observation of ripple migration is possible only in early stages of the experiment, when backlighting can partially penetrate the flow and the accumulating sediment (Fig. 14). In later stages of the experiment, once sediment buildup is too thick to let light penetrate, direct observation of sediment movement is no longer possible. However, the observation of ripples on the surface of the final deposit provides assurance that throughout bed buildup, ripples were migrating across the bed surface (Fig. 15). SEM observations confirmed that the more prominent and uncompacted ripples indeed consist of coarse silt (Fig. 16). Silt of the size range seen in Fig. 16 (coarse to medium silt) is also typical for silt laminae that occur within the sediment layers that accumulated in the flume deposit over the course of the experiments (Fig. 17). These internal silt layers were made visible by letting the sediment in the flume channel dry to a pasty consistency and then scraping a V-shaped trench (Fig. 17) to reveal internal fabrics of deposited sediments (Schieber, 2011). Whereas

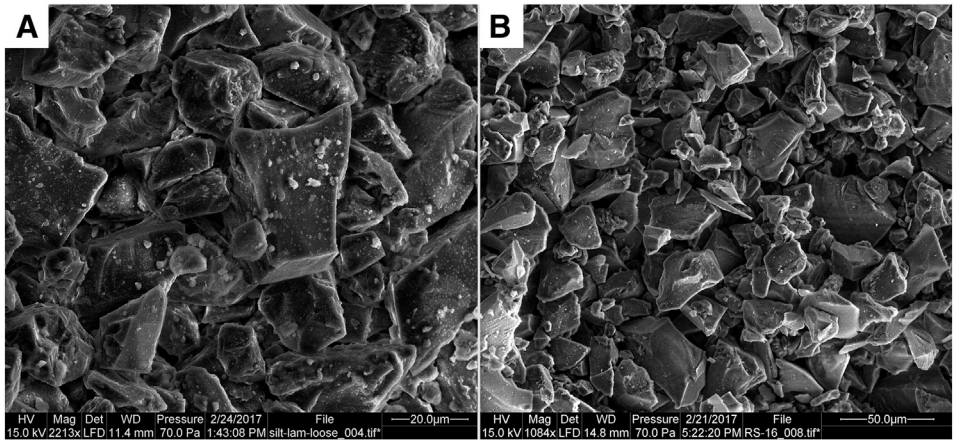

Fig. 16. Typical view (SEM images) of silt grains in silt laminae and silt ripples (Fig. 15) from silt-clay experiments. (A) is from a silt-kaolinite experiment, and (B) is from a silt-illite experiment. These layers typically contain the coarse portion of the added silt component (50 μm top size) as well as a varying proportion of smaller silt grains.

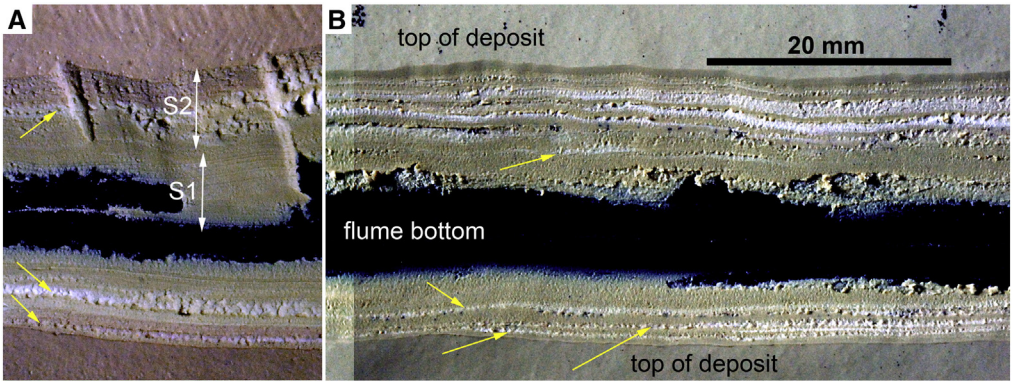

Fig. 17. Images of "Scraped" flume deposit (scrapes oriented parallel to flow direction). Dark center is the flume bottom, gray bands at top and bottom of image are the top of the sediment layer. The area in between is a top view of an oblique cut through the deposit. (A) The initially added sediment mix (deposit marked by double arrow S1) consisted of 5 μm top size quartz silt and illite, and in a second and third stage (deposit marked by double arrow S2) 50 μm top size quartz silt mixed with more illite was added. (B) We observe a laminated deposit where silt layers (bright white, marked with yellow arrows) alternate with beige colored illite layers. Some of the silt layers are lenticular-discontinuous, but most of them are continuous across the field of view and can be followed along the "scrape" for as much as a meter. (For interpretation of the references to colour in this figure legend, the reader is referred to the web version of this article.)

in scrapes parallel to flow direction, silt laminae show considerable lateral continuity (Fig. 17), in exposures perpendicular to flow direction the silt laminae are discontinuous, measuring from less than a centimeter to 5 cm in length (Fig. 18). This observation reflects the fact that silt veneers are laid down by barchans ripples of finite width (Figs. 14, 15).

The interlayering of silt and clay as seen in Figs. 17 and 18 was observed in experiments with silt/kaolinite mixtures, as well as in experiments with silt/illite mixtures. No distinct silt laminae occur in the initial deposits (S1), where only fine silt (5 μm top size) was added. In second-stage deposits (S2) the whitish silt laminae contain abundant coarse silt that is dominated by the top size of the 50 μm quartz silt (Fig. 16). In all silt-clay experiments flow velocity was kept constant (20 cm/s) for the duration of sediment accumulation. The observed interlayering of coarse silt and clay (Figs. 17, 18), and the presence of coarse silt and clay floccule ripples on the same surface (Fig. 15) indicates that the two ripple categories (coarse silt, flocculated clays) were in motion at the same time.

3.4. SEM fabric observations

The quartz-silt component of these experimental sediments spans the range from 50 μm to a few μm. In order to see how the silt sizes are distributed between silty laminae (silt-ripple migration) and clay-rich laminae (floccules-ripple migration), sediment samples were collected from the flume channel in two ways. One method was to collect dried-out flume sediment and argon ion mill (Schieber, 2013; Schieber et al., 2015) it either directly or after infusion with a low-viscosity resin, and then examine it by SEM. Because drying inevitably alters the original depositional fabric, the second method was to collect still wet samples via "coring" with a 10-mm-wide plastic straw, stabilize them with Spurr resin (Schimmelmann et al., 2015), and then argon ion mill them prior to SEM examination. Fig. 19 shows examples from silt-kaolinite experiments.

In all examples (Fig. 19) there is almost no coarse silt in the clay-rich interlayers. Given that about 80% of the quartz silt input is finer than 20 μm (Fig. 6), one wonders thus how the fine silt fraction is "organized" within clay-rich beds. Fig. 20 shows examples of quartz-silt distribution within clay-rich layers from silt-kaolinite experiments.

Fig. 20 illustrates that the clay-rich layers do contain quartz silt, and that the bulk of this matrix hosted quartz silt falls into the 10 μm or smaller size range. Typical clay layers also show a random scattering of somewhat larger silt grains (10–20 μm) that may also be present in coarse-silt layers. In addition to quartz silt in the 10 μm or smaller size range, there are also pieces of kaolinite (booklets) within that size range (Fig. 19B). Both the detrital quartz and the kaolinite booklets appear to be scattered randomly through a matrix of micron-size and smaller clay flakes. The Spurr-resin-stabilized samples preserve the pre-compaction fabric of the flume-deposited muds. The amount of interstitial epoxy documents a high (>80 vol%) initial water content.

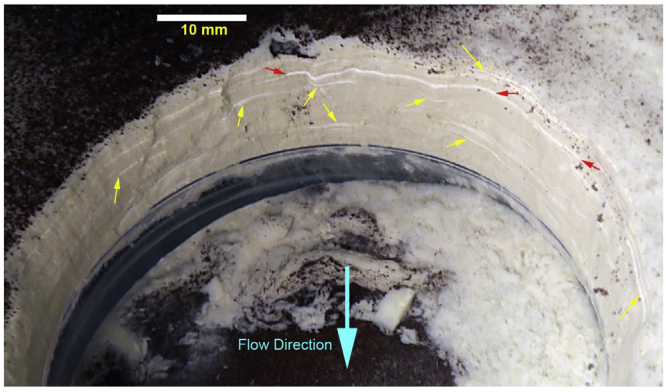

Fig. 18. Flume deposits at the edge of a piston sampler. The piston was moved down to capture a circular sample of the bed, and thus exposed the interior of the bed. This sediment was sub-cored, stabilized with Spurr resin, and ion milled for SEM examination of microfabrics (see Section 3.4). Yellow arrows point to cm-scale discontinuous silt lenses, and red arrows point to a silt lamina that extends for about 5 cm perpendicular to flow direction. (For interpretation of the references to colour in this figure legend, the reader is referred to the web version of this article.)

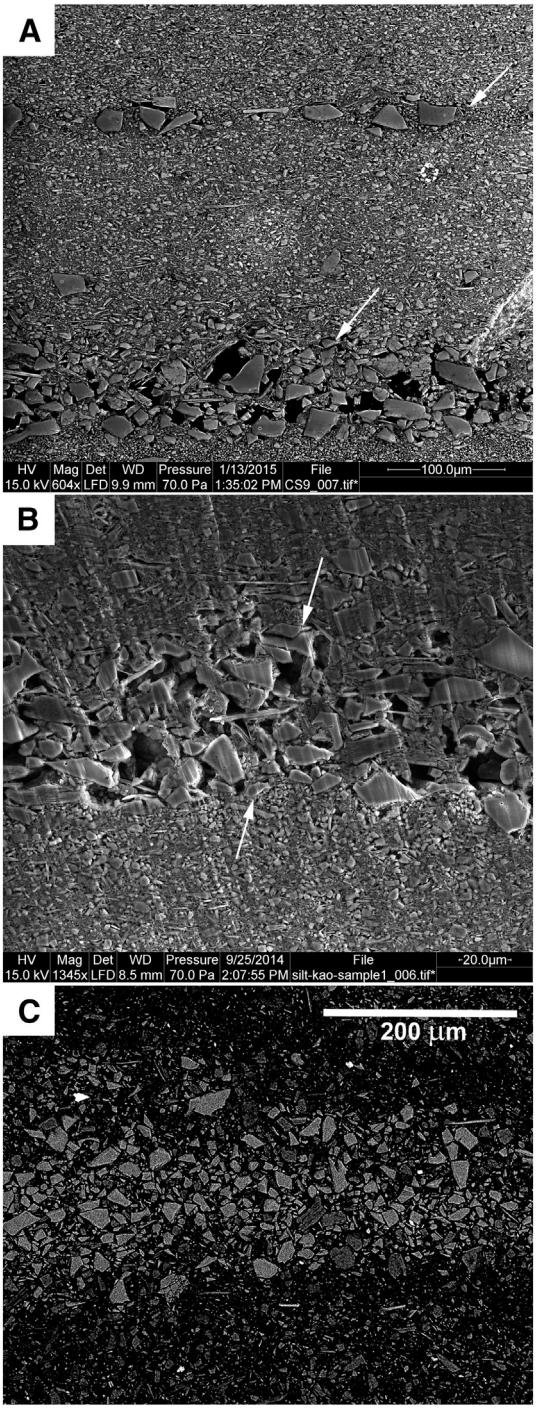

Fig. 19. SEM images of deposits: (A) Dried-out mud with silt laminae (arrows). The coarse silt (tens of μm) is focused on well defined laminae. (B) Closer view of silt lamina (between arrows) from the same sample. Images (A) and (B) were taken in secondary electron mode. (C) Example of a "wet" sample with Spurr resin stabilization, imaged in backscattered electron mode. A lamina of coarse silt is sandwiched between darker and finer sediment. The darker appearance of the latter is due to abundant epoxy resin in the pores (~85% porosity) of the original sediment. The low density of the resin is reflected in low backscatter intensity.

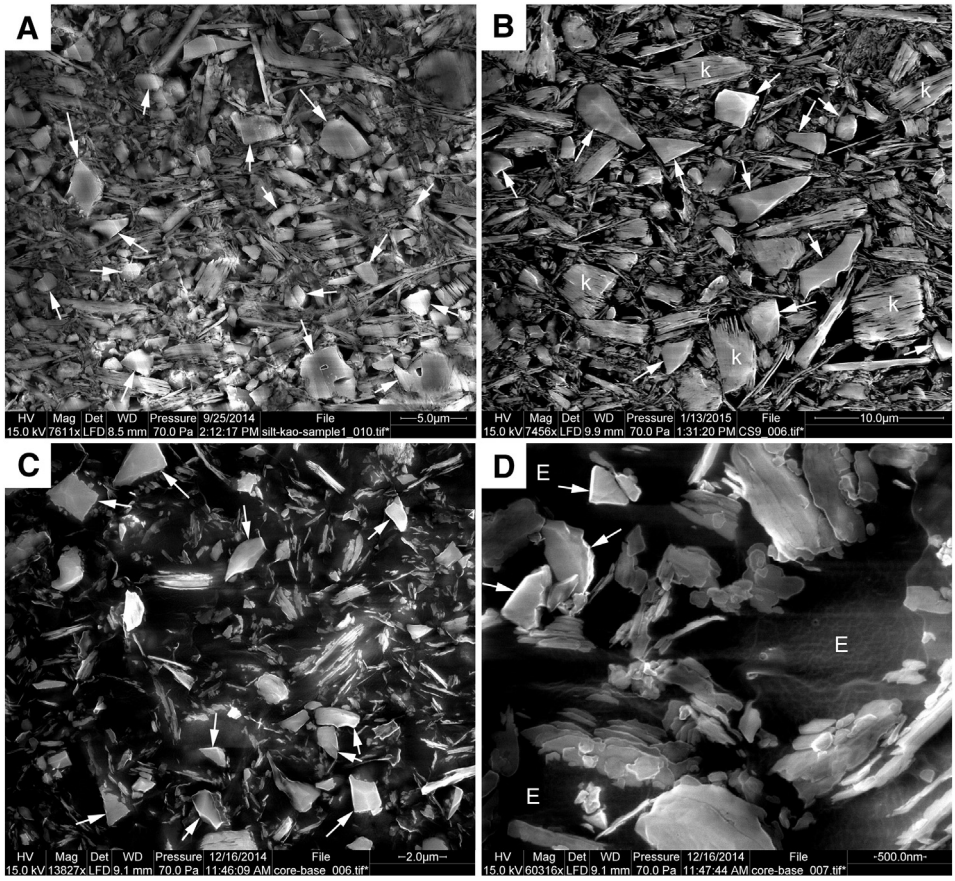

Fig. 20. Quartz silt grains in kaolinite-dominated layers from experiments (SEM images). (A) Air-dried sediment, secondary electron image, quartz grains pointed out by arrows. (B) Air-dried sediment, secondary electron image, quartz grains pointed out by arrows. Note larger kaolinite "booklets" (marked "k") that are about the same size as the quartz grains. (C) "Wet" sample stabilized with Spurr resin. Quartz grains are marked with arrows. Note the random orientation of clay flakes and the random distribution of quartz grains within that matrix. (D) A closer view of the clay matrix within this sample. Randomized network of clay flake chains with larger epoxy-filled pores (marked "E").

The pre-compaction fabric shows randomly oriented clays that form a cardhouse fabric within which the quartz silt grains are "suspended" (Fig. 20C) and linked chains, edge to face, and face to face spatial relationships of clay platelets (Fig. 20D).

Spurr-resin-stabilized samples from the silt-illite experiments show comparable relationships (Fig. 21), although there is added complexity with regard to the nature of silt particles. The lithics seen in the silt-illite samples (Fig. 21) are due to the fact that commercially available clays are in essence finely ground shales, and that the source material rarely completely disintegrates into clay flakes. Commercial clays therefore typically contain a proportion of source-material rock fragments that are in the silt size range (62.5 μm and smaller). The kaolinite booklets in Fig. 20 are the same thing, coarser fragments of a ground-up clay deposit. However, for understanding the partitioning of silt particles between silt ripples and floccule ripples it does not really matter what the silt grains are made of as long as they have comparable densities. Given that quartz, illite, and kaolinite particles are within a few percent of each other with regard to density (Correns, 1969) they are apt to show comparable behavior during fluid transport. Thus, Fig. 21, Spurr-resin-embedded "wet" samples from silt-illite experiments illustrate the same features that Fig. 20 illustrated for silt-kaolinite experiments. The images show the pre-compaction fabric of flume-deposited muds and document a high initial water content (space now filled with epoxy). Silt grains (lithics and quartz) that are typically 10 μm or smaller are randomly scattered and "suspended" in a matrix of micron-size and smaller clay flakes. The latter are randomly oriented and show a cardhouse fabric with linked chains, edge to face, and face to face spatial relationships of clay platelets.

4. Discussion

The textural characteristics of the clay fabrics shown in Figs. 20 and 21 are common for flocculated clays (e.g. Bennett et al., 1990) and confirm the assumptions reached on the basis of observing large flocculated aggregates in the course of these experiments (Fig. 15), as well as in precursor experiments (Schieber et al., 2007, 2013). As outlined in the introduction, silt-laminated shales (or mudstones) are common in the rock record and due to their ubiquity have attracted multiple attempts to interpret them as the outcome of specific processes or environments (Kemp, 1996; Potter et al., 2005; Lazar et al., 2015). When looked at in detail there are multiple styles of lamination (Schieber, 1990; O'Brien, 1996), and it is obvious that depending on these details multiple causes and processes apply. Among the mechanisms that have been proposed for the generation of silt laminae in muds are pulsating currents (e.g. Lombard, 1963; Lambert et al., 1976), stacking of multiple depositional events with varying energy (Moore, 1969; O'Brien, 1989), reworking by bottom currents (Hollister, 1967), and congregational sorting (Piper, 1972). In terms of actual transport events these "mechanisms" can probably considered subtle variations on the same theme, moving mud and muddy suspensions with flowing currents. To actually "read" the differences from laminae in the rock record poses a formidable challenge and should probably be explored further through experimental studies. The focus in this study is on one particular case, non-graded silt laminae, a few grains thick (Fig. 19), with sharp boundaries to underlying and overlying muds, and specifically those that show some kind of association with lens formation (Fig. 4) and bona-fide ripples (Fig. 2). Although explored here via experiments with unidirectional

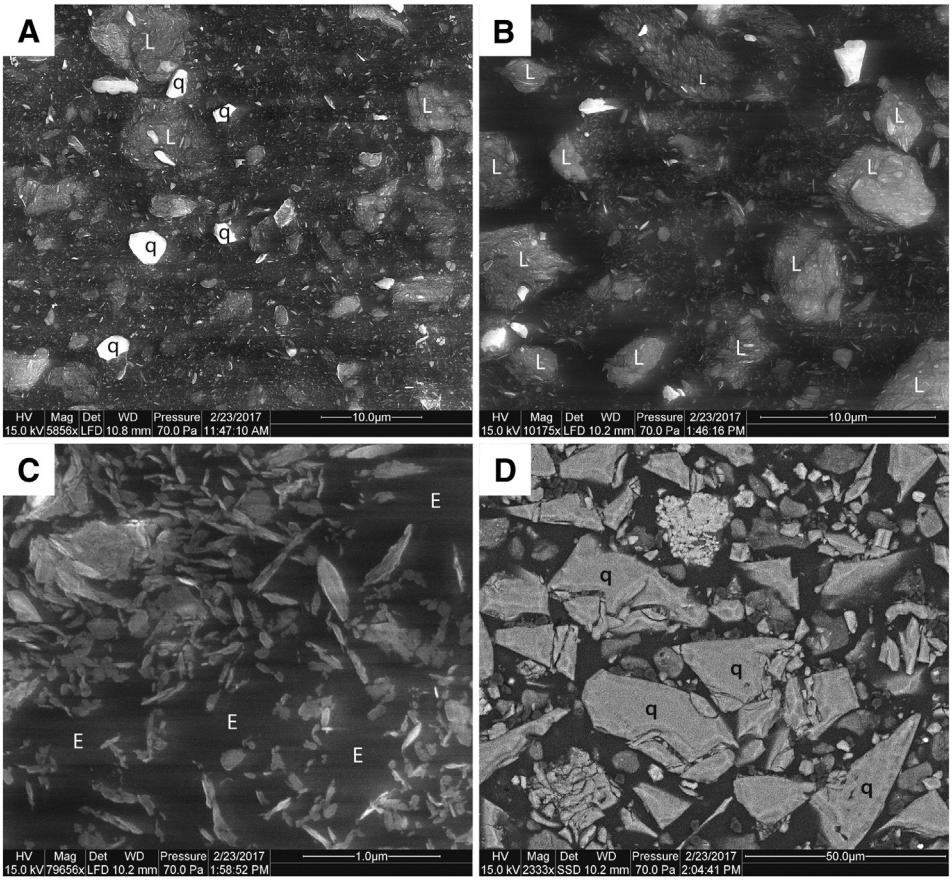

Fig. 21. SEM images of grain-scale sedimentary fabrics as seen in a silt-illite experiment, from a water-saturated sample that was stabilized with Spurr resin (Schimmelmann et al., 2015). (A) Microfabric of a clay-dominated layer shows larger particles suspended in a finer matrix. The "larger" (5–10 μm) particles are quartz grains (q) as well as (L) shale lithics (original shale clasts; sensu Schieber, 2016). (B) A closer view of the fabric shown in part A. It shows that the lithics (L) are surrounded by a matrix of randomly oriented clay flakes. (C) A close-up of the clay fabric from part B that shows a large amount of intergranular porosity that is filled with dark epoxy resin (E). (D) Close-up of a coarse silt lamina for comparison (note lower magnification). The lamina is dominated by quartz silt (q) grains that measure several 10 μm size. Some of the quartz grains were fractured during sectioning of the sample with a diamond wafering saw.

currents, wave and tide generated currents that reach the critical velocities could conceivable also produce ripple-related laminae. How these might differ in detail from laminae produced under unidirectional currents is currently unknown, but a topic we plan to explore with a newly built flume that can reproduce tidal and wave generated currents. Because wave action and tides invariably influence the current systems of marine shelf seas, such experiments may eventually allow us to identify and differentiate lamina styles that reflect unidirectional, tide dominated, and wave influenced flow regimes in the rock record. With regard to laminae that are only a few grains thick (Figs. 1, 4, 19) it has in the past been suggested that these are likely deposits of hemipelagic suspensions or eolian input (O'Brien, 1989), what is described here suggests an alternative interpretation.

The sediment (clay plus silt) was added as a mixture and at a high degree of turbulence (flow velocity 50 cm/s; 5 cm effective flow depth), and thus it is conceivable that early-formed fluid-borne floccules consisted of a mixture of all the components that were swirling around in suspension. It is of course not a given that fluid borne floccules actually consist of a mixture of all particles in turbulent suspension. And if so, one should probably consider whether the larger silt grains, due to their much higher density, might not simply "settle out" of these flocs, arrive at the bed first, and then form discrete silt ripples. Whereas these issues were unresolved when we started this study, a recent experimental investigation on the settling behavior of clay and silt mixtures (Tran and Strom, 2017), confirms our initial assumptions. These authors (Tran and Strom, 2017) found that most of the silt in turbulent suspensions (regardless of size) was indeed incorporated in clay-dominated floccules, and by extension this means that if such floccules settled to the bed they would have contained large silt grains at the time of arrival.

What we observed once velocity was lowered to the point that clay floccules could travel and accumulate in bedload (Schieber et al., 2007), was that coarse silt became segregated and travelled as ripples that stayed separate from ripples consisting of flocculated clays. A comparable phenomenon of silt from clay segregation has been called upon to explain the formation of alternating silt-clay laminae in fine-grained turbidity currents (Stow and Bowen, 1980). The latter authors proposed that depositional sorting by increased shear in the boundary layer led to destruction of clay flocs and allowed only silt grains to settle to the bottom and form a silt layer.

In our experiments, however, the near-bed shear is sufficiently small that flocculated clays can settle to the bottom and become bedload particles. The floccules are not destroyed, and clays are not removed and returned to the flow, and thus an alternative mechanism for separating coarse silt from clay is needed. If one looks at Figs. 20 and 21, and considers (a) that floccules are on the order of 100 to 200 μm in size, and (b) that the matrix images only show a 40 by 40 μm area, all of these frames are likely from the interior of floccules.

What we also see in these images is that small silt grains (10 μm or smaller) are rather common in floccules. By extension one might also surmise that larger silt grains might also have been incorporated into floccules as long as these were moving with the fluid in the main body of the flow. Once in bedload, however, the rolling and tumbling motion of the floccules (easily observed from beneath the flume) is likely to

have caused significant velocity changes that induced floccules to break up and release large silt grains. If we assume for a moment a 100 μm diameter floccule (80 vol% water content) that includes a 50 μm silt grain, the silt grain contributes 40% of the total mass yet only occupies 14% of the volume. We have a fragile cardhouse where nearly half the mass is concentrated in a small area within a substantially larger structure. One can surmise that the inertia of this concentrated mass will stress and potentially break the floccule structure every time there is a change of direction and velocity, such as induced by tumbling and bouncing over the bed or flume bottom. How this may lead to segregation of coarse silt from the flocculated bedload is sketched out in Fig. 22.

Direct observations from our experiments support the inferences made in Fig. 22 because they document that coarse silt and floccules ripples migrate over the same surface at the same time (Fig. 15). These observations further document that after some time interval of floccule breakage and silt segregation two distinct types of ripples migrated through the flume channel. Given the observation that both floccules ripples and silt ripples leave behind a thin veneer of sediment (Figs. 11, 12, and 13), continued ripple migration will necessarily build up a deposit that consists of stacked silt and clay "tails" and thus forms a silt-laminated mud bed (Fig. 23).

The model in Fig. 23 is an idealized situation. The "continuous" laminae that it depicts should not be expected to extend indefinitely in either flume or natural settings. Transverse forms (Fig. 23) can in principle produce laterally extensive sheets of silt, but would have to migrate long distances without changing form and would need to be resupplied with sediment or else die out. It is difficult enough to maintain these conditions in a flume and in nature it appears unlikely that they could be maintained for long. In nature, unlike in our experiments, it is likely that flow velocities will fluctuate, causing for example

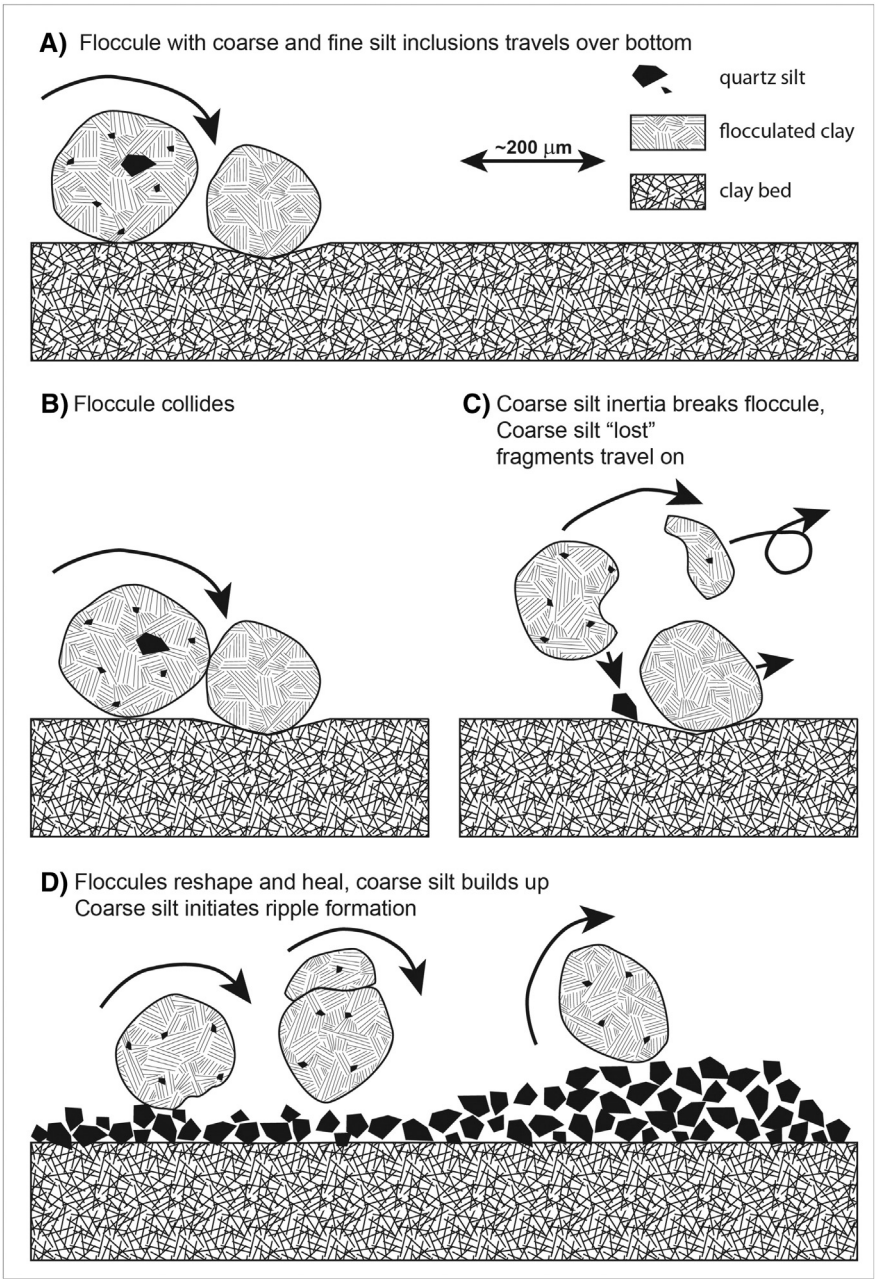

Fig. 22. Model for the separation of coarse silt from bedload floccules. (A) Coarse-silt-bearing clay floccule travels over the bed and encounters an obstacle. (B) Collision with obstacle causes slowdown of floccule; inertial forces of quartz grain cause breakage of floccule. (C) Floccule fragments move on in the current, and coarse silt grain settles to the bottom. (D) Coarse silt builds up and starts to form silt ripples that migrate over the bed surface. Simultaneously, clay floccules with inclusions of small silt grains grow to equilibrium size and form migrating floccule ripples.

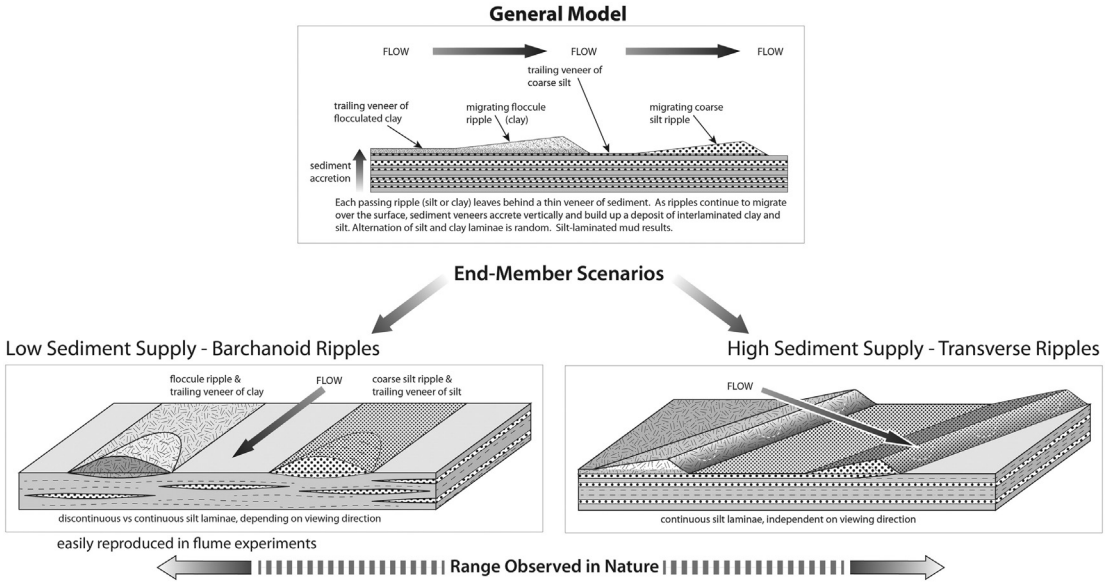

Fig. 23. Conceptual view of the origin of interlaminated coarse silt and mud. Coarse-silt ripples and clay-floccule ripples migrate over the same surface. Over time, any given point on that surface will be traversed by a random succession of silt and floccules (clay) ripples, and the sediment veneers they leave behind will accumulate into a laminated deposit. The continuity of these laminae will depend on ripple geometry (barchans vs. transverse) and thus on sedimentation rate. Two end-member scenarios are shown, with (1) only barchans on the left, producing discontinuous laminae in views perpendicular to flow direction, and (2) only transverse ripples on the right, producing continuous laminae in all viewing directions.

intermittent non-deposition or even erosion and scouring. Variable sedimentation rates also influence the appearance of the accumulating deposit. For example, when sedimentation rates are low the migrating ripples likely will only leave behind a very thin residuum, whereas at times of high sedimentation rates not just a sediment veneer but an entire ripple might be preserved. This difference is for example exemplified by the rock-record examples shown in Fig. 1 (low sedimentation rate) and Fig. 2 (high sedimentation rate). With regard to flume observations, high-sedimentation-rate scenarios (Fig. 23, bottom right) are much more difficult to sustain in a flume experiment than low-sedimentation-rate scenarios (Fig. 23, bottom left). Because of these inherent difficulties our flume observations (Figs. 14, 15, 17, 18) largely validate the low sedimentation rate scenarios. Nonetheless, in natural deposits we see the entire range of lamina styles (discontinuous to continuous) that is covered between the Fig. 23 end members (Figs. 1, 2, 3, 4), something to be expected in sediment intervals that span thousands of years of accumulation and inevitable shifts of depositional parameters. Thus, at the scale of thin sections and hand specimens the envisioned model does explain the observed laminae, but flume observations suggest that lateral continuity should not be expected to exceed a few meters.

An important demarcation in this context is the critical velocity of sedimentation for the clay floccules (Schieber et al., 2007). For typical clays (kaolinite, illite, smectite) this marker is located approximately at 25 cm/s (Schieber et al., 2007; Schieber and Southard, 2009; Schieber and Yawar, 2009; Schieber, 2011), and at velocities above it we should only expect laminated silts, whereas at velocities below it we should expect interlaminated silt and clay (Fig. 24).

The envisioned model of mud deposition also provides a mechanistic explanation for the partitioning of coarse silt (62–20 μm) and fine silt (20–2 μm) during deposition. The fine silt is integrated ("soaked up") into clay floccules because it does not lead to their destruction during transport, and the coarse silt segregates for that very reason and forms separate deposits (Fig. 22). Observing that the matrix quartz is for the most part smaller than 20 μm and dominantly 10 μm and smaller is of

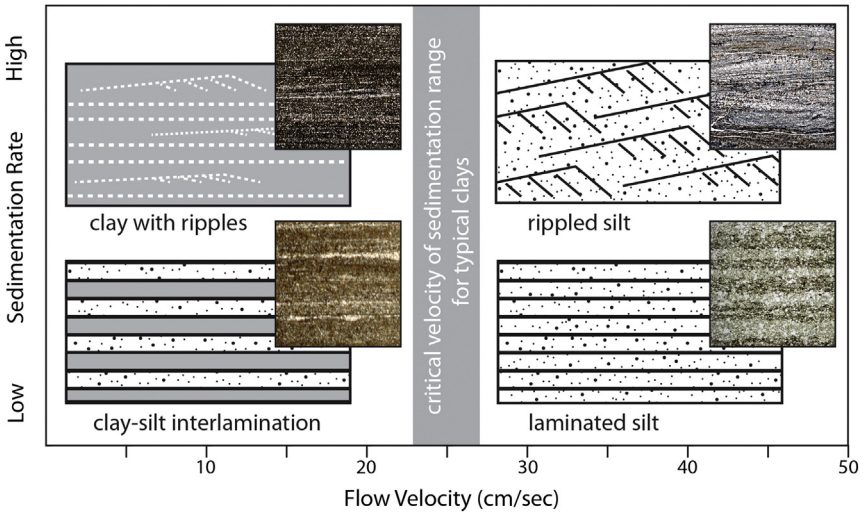

Fig. 24. A conceptual view of envisioned textural changes in relation to flow velocity and sedimentation rate. The photomicrograph insets are all of similar scale, and represent sub-frames of 5–7 mm width.

some interest, because that is also the typical grain size range for eolian dust that can be transported over large distances and deposited in ocean basins (Nickling and McKenna Neuman, 2009). Although scattered fine silt grains in shales have on occasion be attributed to eolian input (e.g. Sageman et al., 2003; Pike and Kemp, 1996; O'Brien, 1996), incorporating fine silt into floccules during transport offers an alternative explanation.

5. Conclusion

When turbid suspensions of silt and clays are propelled through a flume at flow velocities of 25 cm/s or less, both silt and clay travel in bedload in the form of ripples. Even though a thoroughly mixed sediment is added to the flow, quartz silt separates from clays and silt ripples and clay-floccule ripples migrate downcurrent as discrete entities. Not all the silt, however, ends up in silt ripples. Silt ripples are dominated by grain sizes in the 62 to 30 μm range, whereas the large amount of fine silt (20 to 2 μm) that was added to our experiments is largely blended in with the clays. A model is proposed where coarse silt destabilizes floccules and accumulates separately at the bed surface, whereas fine silt is incorporated into clay floccules and becomes part of the mudstone matrix. As both types of ripples migrate over the bed they leave behind thin veneers of sediment, and as multiple ripples migrate over the same spot a randomly interlaminated deposit of clay (with fine silt) and coarse silt builds up. The proposed model also predicts a systematic arrangement of certain mudstone textures (interlaminated silt and mud, laminated silt, ripple laminated mud, rippled silt, continuous vs discontinuous laminae) as a consequence of flow velocity and relative sedimentation rates. Such a model should be helpful for the interpretation mudstone paleoenvironments.

Acknowledgements

This research project was supported by the Indiana University Shale Research Consortium (sponsored by ExxonMobil, Chevron, Shell Oil, Anadarko Petroleum, Marathon Oil, Wintershall, Whiting Petroleum, ConcoPhillips, and Statoil). Funds for construction of the flumes used in the experiments were provided by the National Science Foundation under award numbers EAR0617128, EAR0308921, and OCE0930829. Comments by Chris Paola on an earlier version of the manuscript, as well as suggestions by an anonymous reviewer and Journal Editor Brian Jones, helped to improve the structure and readability of the final manuscript.

References

Bennett, R.H., O'Brien, N.R., Hulbert, M.H., 1990. Determinants of clay and shale microfabric signatures: processes and mechanisms. In: Bennet, R.H., Bryant, W.R., Hulbert (Eds.), Microstructure of Fine-Grained Sediments. Springer Verlag, New York, pp. 5–32.
Blatt, H., 1982. Sedimentary Petrology. W.H. Freeman & Co., New York, N.Y. (564 pp.).
Cluff, R.M., 1980. Paleoenvironment of the New Albany Shale Group (Devonian-Mississippian) of Illinois. Journal of Sedimentary Petrology 5, 767–778.
Correns, C.W., 1969. Introduction to Mineralogy. Springer Verlag, Berlin (485 pp.).
Haines, J., Mazullo, J., 1988. The original shapes of quartz silt grains: a test of the validity of the use of quartz grain shape analysis to determine the sources of terrigenous silt in marine sedimentary deposits. Marine Geology 78, 227–240.
Hollister, D., 1967. Sediment Distribution and Deep Circulation in the Western North Atlantic. (Unpublished Ph. D. Thesis). Columbia University.
Jopling, A.V., Forbes, D.L., 1979. Flume study of silt transportation and deposition. Geografiska Annaler. Series A, Physical Geography 61, 67–85.
Kemp, A.E.S., 1996. Palaecolimatology and Palaeoceanography from Laminated Sediments. Geological Society Special Publication, London v. 116.
Lambert, A.M., Kelts, K.R., Marshall, N.F, 1976. Measurements of density underflows from Walensee, Switzerland. Sedimentology 23, 87–105.
Lazar, R., Bohacs, K.M., Schieber, J., Macquaker, J., Demko, T., 2015. Mudstone primer: Lithofacies variations, diagnostic criteria, and sedimentologic/stratigraphic implications at lamina to bedset scale. SEPM Concepts in Sedimentology and Paleontology #12 (198 pp.).
Lombard, A., 1963. Laminites: a structure of flysh/type sediments. Journal of Sedimentary Petrology 33, 14–22.
Lundegard, P.D., Samuels, N.D., 1980. Field classification of fine-grained sedimentary rocks. Journal of Sedimentary Petrology 50, 781–786.
Mantz, P.A., 1978. Bedforms produced by fine, cohesionless, granular and flakey sediments under subcritical water flows. Sedimentology 25, 83–103.
Milliken, K., Choh, S.-J., Papazis, P., Schieber, J., 2007. "Cherty" stringers in the Barnett Shale are agglutinated foraminifera. Sedimentary Geology 198, 221–232.
Moore, D.G, 1969. Reflection profiling studies on the California Borderland: structure and Quaternary turbidite basins. Geological Society of America, Special Paper 107 142.
Nickling, W.G., McKenna Neuman, C., 2009. Aeolian sediment transport. In: Parsons, A., Abrahams, A.D. (Eds.), Geomorphology of Desert Environments, pp. 517–555.
Nuhfer, E.B., 1981. Mudrock fabrics and their significance: discussion. Journal of Sedimentary Petrology 51, 1027–1029.
O'Brien, N.R., 1989. The origin of lamination in middle and upper Devonian black shales, New York state. Northeastern Geology 11, 159–165.
O'Brien, N.R., 1996. Shale lamination and sedimentary processes. Geological Society of London Special Publication, London 116, 23–36.
Pike, J., Kemp, A.E.S., 1996. Records of seasonal flux in Holocene laminated sediments from the Gulf of California. Geological Society Special Publication, London 116, 157–169.
Piper, D.J.W., 1972. Turbidite origin of some laminated mudstones. Geological Magazine 109, 115–126.
Potter, P.E., Maynard, J.B., Pryor, W.A., 1980. Sedimentology of Shale - Study Guide and Reference Source. Springer, New York, N.Y. (306 pp.).
Potter, P.E., Maynard, J.B., Depetris, P.J., 2005. Mud and Mudstones: Introduction and Overview. Springer-Verlag, Berlin, Heidelberg, New York (297 pp.).
Pye, K., 1994. Shape sorting during wind transport of quartz silt grains – discussion. Journal of Sedimentary Research A64, 704–705.
Rees, A.I., 1966. Some flume experiments with a fine silt. Sedimentology 6, 209–240.
Sageman, B.B., Murphy, A.E., Werne, J.P., Ver Straeten, C.A., Hollander, D.J., Lyons, T.W., 2003. A tale of shales. The relative roles of production, decomposition, and dilution in the accumulation of organic-rich strata, Middle–Upper Devonian, Appalachian basin. Chemical Geology 195, 229–273.
Schieber, J., 1990. Significance of styles of epicontinental shale sedimentation in the belt basin, mid-Proterozoic of Montana, U.S.A. Sedimentary Geology 69, 297–312.
Schieber, J., 2009. Discovery of agglutinated benthic foraminifera in Devonian black shales and their relevance for the redox state of ancient seas. Palaeogeography, Palaeoclimatology, Palaeoecology 271, 292–300.
Schieber, J., 2011. Reverse engineering mother nature – shale sedimentology from an experimental perspective. Sedimentary Geology 238, 1–22.
Schieber, J., 2013. SEM observations on ion-milled samples of Devonian black shales from Indiana and New York: the petrographic context of multiple pore types. AAPG Memoir 102, 153–172.
Schieber, J., 2016. Experimental testing of the transport-durability of shale Lithics and its implications for interpreting the rock record. Sedimentary Geology 331, 162–169.
Schieber, J., Southard, J.B., 2009. Bedload transport of mud by floccule ripples – direct observation of ripple migration processes and their implications. Geology 37, 483–486.
Schieber, J., Yawar, Z., 2009. A new twist on mud deposition - mud ripples in experiment and rock record. The Sedimentary Record 7, 4–8.
Schieber, J., Krinsley, D., Riciputi, L., 2000. Diagenetic origin of quartz silt in mudstones and implications for silica cycling. Nature 406, 981–985.
Schieber, J., Southard, J.B., Thaisen, K.G., 2007. Accretion of mudstone beds from migrating floccule ripples. Science 318, 1760–1763 (December 14).
Schieber, J., Southard, J.B., Kissling, P., Rossman, B., Ginsburg, R., 2013. Experimental deposition of carbonate mud from moving suspensions: importance of flocculation and implications for modern and ancient carbonate mud deposition. Journal of Sedimentary Research 83, 1025–1031.
Schieber, J., Lazar, R., Bohacs, K., Klimentidis, B., Ottmann, J., Dumitrescu, M., 2015. An SEM study of porosity in the eagle ford shale of Texas – pore types and porosity distribution in a depositional and sequence stratigraphic context. AAPG Memoir 110, 153–172.
Schimmelmann, A., Riese, David J., Schieber, Juergen, 2015. Fast and economical sampling and resin-embedding technique for small cores of unconsolidated, fine-grained sediment. 2015 Pacific Climate (PACLIM) Workshop, 8–11 March, Asilomar Conference Grounds, Pacific Grove, California, pp. 50–51 (abstracts).
Stow, D.A.V., Bowen, A.J., 1980. A physical model for the transport and sorting of fine-grained sediments by turbidity currents. Sedimentology 27, 31–46.
Tran, D., Strom, K., 2017. Suspended clays and silts: are they independent or dependent fractions when it comes to settling in a turbulent suspension. Continental Shelf Research 138, 81–94.
Ulmer-Scholle, D.S., Scholle, P.A., Schieber, J., Raine, R.J., 2015. A color guide to the petrography of sandstones, siltstones, shales and associated rocks. AAPG Memoir 109 (509 pp.).